DS Journal of Digital Science and Technology
Volume 4 Issue 2, 69-86, Apr - Jun 2025
ISSN: 2583-5416/ https://doi.org/10.59232/DST-V4I2P105

Original Article

Identification and Segmentation of Renal Cancer Using MSRNet-3D and SAS Optimization in 3D-CT Imaging

Swapna J[1], Roselin Kiruba R [2]

[1,2]*Department of Computer Science and Engineering,*
Vel Tech Rangarajan Dr. Sagunthala R&D Institute of Science and Technology, Tamil Nadu, India.

[1]swapnabinesh27@gmail.com

Received: 10 April 2025; Revised: 15 May 2025; Accepted: 10 June 2025; Published: 30 June 2025

Abstract - Since renal cancer is a major worldwide health concern, lowering mortality and hospitalization rates necessitates early detection and identification. By providing physicians with comprehensive anatomical information essential for tumour location and characterisation, the enlargement of Three-Dimensional Computed Tomography (3D-CT) has completely changed the diagnosis of renal malignancies. In order to improve overall diagnostics precision and effectiveness, sophisticated deep learning tactics are currently being developed to take into account the intricate forms of tumours and the artifacts created throughout imaging. However, there are many drawbacks to the present techniques for renal carcinoma classification, such as their high computing requirements, noise sensitivity, and unpredictability in tumour form. Introduce a new deep learning approach called Multi-Scale RenalNet 3D (MSRNet-3D) to address these issues and improve the classification of renal cancer in 3D-CT scans. To improve segmentation accuracy and resilience, MSRNet-3D incorporates multi-scale along with multi-level convolutional networks into its framework. The Seahorse Adaptive Search Optimization (SAAO) methodology, which adjusts model variables to promote rapid convergence and solve training-related issues, is an important invention of this work. The outcomes show notable gains in computational effectiveness, robustness against tumour variance, and segmentation accuracy. The crucial distinction between the establishment of Artificial Intelligence (AI)-based techniques for accurate renal cancer diagnosis and treatment planning and recent advances in imaging technology is addressed in the current research. When it came to the segmentation of renal carcinoma from 3D-CT scans, the MSRNet-3D model proposed in this research performed well. According to experimental results, the model's unmatched capacity for tumour detection and delineation to an exceptionally high level of precision is established by its 99% accuracy rate, 98.9% accuracy, and 99% recall. MSRNet-3D's F1-score, which gauges performance in terms of recall and accuracy, was 98.8%.

Keywords - 3D image segmentation, Renal cancer, Cancer identification, Medical imaging, 3D Computed Tomography (3D-CT), Deep Learning (DL).

1. Introduction

Since renal carcinoma is among the most prevalent ten cancers worldwide, early identification increases the likelihood of mortality and allows for effective therapy [1, 2]. Since renal cancer therapy frequently yields positive results and prolongs survival, identifying it early can significantly increase the likelihood of successful therapy. Early renal cancer identification and diagnosis depend comprehensively on imaging, particularly when using Computed Tomography (CT) imaging. In order to identify and accurately diagnose cancer with its earliest indications and symptoms, CT imaging furthermore offers incredibly precise images of internal and abdominal

tissues. Renal tumour quantities, regions, and contours are clearly visible on CT imaging [3]. In order to make a diagnosis and develop a plan for therapy, it is essential to define these qualities clinically. Renal Cell Carcinoma (RCC) is the only type of cancer of the renal cells among the many tumours in the renals; RCCs are tumours in and of themselves because they are responsible for the majority of related morbidities and deaths [4].

A better clinical course is usually conveyed by the tumours of chromophobe RCC, a significantly unusual histological category. Since oncocytomas are typically benign tumours and cannot be distinguished from malignant histopathological subcategories of RCC, they exhibit more sluggish behaviour [5]. Ten to fifteen percent of RCC is papillary RCC. Subgroups have been categorized into types 1 and 2 based on variations in histological structure and clinical characteristics. In the clinical context, renal tumour histologic subtyping is significant. Precise classification ensures the best possible treatment plans and eliminates unnecessary biopsies or operations. For instance, separating benign RCC versus oncocytomas will prevent unnecessary surgery and lower patient mortality [6]. Conversely, early detection of persistent RCC subtypes may help direct more focused and timely treatment approaches, which are more likely to influence patient outcomes. Medical imaging contributes to more than simply the first diagnosis, as well as the identification of renal cancer. Numerous characteristics of the tumour and its surroundings, such as its size, shape, and progression patterns, may now be examined thanks to the advancements in imaging methods and algorithms for processing images [7, 8]. When preparing for surgery or other interventional procedures, the data is crucial for tracking and assessing the response to therapy. It makes it possible to evaluate the tumour volume with great precision and detect minute temporal shifts, both of which are important for modifying treatment.

Globally, renal cancer is a substantial and consistent risk factor for health. Improved survival probability, accomplished by early identification, is the main predictable factor determining successful therapy. The early diagnosis of renal cancers and thorough research on them are significantly aided by medical imaging using CT [9]. Essential milestones in the clinical evaluation and treatment strategy of individuals with renal cancer include renal tumour segmentation [9] and precise tumour identification. With such accurate histopathology, the categorization of this new imaging procedure can help clinicians treat patients with renal cancer more effectively, preventing needless procedures and eventually improving patient outcomes. Imaging technology alternatives and computational methodologies have great promise for greatly enhancing the precision and dependability of renal cancer identification and treatment. In the analysis of medical images, clinical 3D segmentation of images [10] is a crucial procedure that is key to numerous applications, ranging from therapeutic planning to diagnosis. Segmentation is the process of dividing a 3D medical image into distinct areas that correspond to distinct pathogenic individuals or anatomical components, primarily organs, tissues, or malignancies. Its complete goal is to determine a diagnosis or action by accurately identifying such locations for additional investigation. In addition to the presumption, clinical 3D image classification is known for its high accuracy [11].

- The goal of this research is to create a novel approach called MSRNet-3D that will enable reliable and precise renal carcinoma segmentation from 3D-CT scans.
- It also aims to develop sophisticated Deep Learning (DL) based segmentation along with diagnosis tools for renal cancer illness.
- Additionally, to identify the weight degradation factor of segmentation and improve its overall recognition efficiency, the Seahorse Adaptive Search (SAS) optimization is used.
- Compared to conventional approaches used for identifying and categorising renal cancer, a thorough performance analysis is carried out that will significantly surpass the effectiveness and resilience of the constructed model for MSRNet-3D.

2. Related Works

A number of sophisticated algorithms intended to enhance the accuracy and dependability of renal cancer recognition, aided by methods utilizing DL and enhanced computational approaches, have been addressed in this

chapter, along with a brief description and a critical assessment of fresh approaches to segmentation employed in identifying renal malignancies. In order to determine their effectiveness at the level of therapy, it would be feasible to acquire different metrics from every approach, such as segmentation precision, specificity, sensitivity, computational effectiveness, etc. In [12], it was pointed out that CT texture feature evaluation might produce an accurate destructive classification, analyze prognosis, and genome genetic type in cancer of renal cells.

In order to estimate the clinical consequences, the focus will be placed on computing methods for radiomic aspects of CT images, such as the distinction of different types among pure cell RCC, polymorphic RCC, with chromophobe RCC, as well as key prognostic factors and genomic characteristics [13]. This might have been done to analyze CT scan texture characteristics to comprehend tissue variability. It is an evaluation event that affects how patients with RCC are diagnosed and treated. The comprehension and treatment of RCC may be enhanced by these unobtrusive radiomic indicators. One of the earliest methods for addressing difficulties in renal cancer diagnosis with contemporary AI technologies is presented in [14]. Their research proposes the creation of a single end-to-end automated framework to reduce the amount of manual labour involved in renal mass and segmentation [15].

In order to isolate areas of interest, the sophisticated approaches at the core of this structure start using a 3D renal and tumour segmentation framework depending on the 3D-UNet design, which examines 3D CT scans and precisely segments sections of the renal and tumours [16]. A multi-level feature extraction tool is added to allow for thorough characterisation of the segmented areas. Furthermore, it incorporates an XGBoost procedure predicting classifier to enable well-informed judgments regarding the recommendation of a partial or complete radical nephrectomy depending on the segmentation characteristics [17]. Last but not least, a strong five-fold replication strategy at the framework level guarantees that precise renal cancer detection and mitigation strategies are implemented in actual clinical settings. Reviewing recent advancements in AI's application to the assessment of renal cancer, along with estimating its significant influence on medical evaluation and treatment, is the goal of [18]. It estimates how well AI-powered technologies can interpret intricate medical images to detect illnesses early on and change the course of sick people's lives. It talks about some possible directions for future research and improvement in AI, machine learning, and DL, all of which are essential for enhancing medical planning and accuracy in diagnosis. Additionally, it highlights particular difficulties or limitations associated with using these advancements in clinical settings. This highlights the need for constant innovation and the utilization of AI to improve healthcare practices further [19].

In [20], a DL framework was established throughout its entirety for heterogeneous classification of the five major renal tumour histopathological categories with normal and dangerous tumours by multi-phase CT. Within one structure, tumours will be recognized, and tumour classifications will be recognized without manual operator interference. Employing DL approaches will automate the diagnosis technique and likely enhance precision and effectiveness in medical environments. [21] offers models for detecting renal cancers with CT. It suggests three models for detecting renal tumours: VGG16, ResNet50, and a two-dimensional convolutional neural network containing six layers. These simulations are meant for assessing the CT scan for any indications of a renal tumour, utilizing their depths and characteristics that help obtain exceptional detection reliability.

The primary research constraints in the identification of renal carcinoma disease are associated with modern segmentation techniques [22]. Strong models that can accurately define the fundamental variations of tumour images across various stages and patient characteristics are needed, even though initial attempts employing DL and specialized categories like UNet, ResNet, among others have achieved significant strides in this task. These methods typically reduce the capacity of current methodologies to adapt to diversity in tumour forms, sizes, and textures because they transfer extremely poorly to practical problems of diagnostic precision. Systems for clinical decision-support must use enhanced approaches to segmentation to enhance hospital treatment strategy and diagnostics operations. Most models created for this task concentrate on segmentation and cannot be easily

integrated into the clinic's larger workflow or context. DL models [23] for renal cancer segmentation ought to have interpretability and clarity to be accepted in medical care, which has not been fully investigated. Clear information about the model's decision-making process would increase healthcare practitioners' confidence in it and make it easier to incorporate it into standard clinical practice.

It suggests creating a DL platform throughout its entirety DL platform in order to close these gaps. Comprehensible results and smooth interaction with systems for clinical decision support enhance the precision of segmentation along with clinical use [24, 25]. This research emphasizes enhancing model resilience, scalability with various datasets, and comprehension in order to close the gap between AI research and clinical practice. Research is further motivated by the possibility of significantly lowering diagnostic mistakes and improving the preparation of treatments for better patient outcomes through more precise and effective renal cancer identification and characterisation. This suggests a research gap from the examined literature, highlighting the need for approaches to algorithms for segmentation that appropriately account for computing limitations, imaging noise, and tumour shape diversity.

This methodology also emphasizes scalability to various datasets, varying by imaging variance or data heterogeneity, to guarantee that the models stay strong and dependable. Since a model must function consistently across many hospitals, scanners, and populations, scalability is essential to clinical translation. The precision of renal cancer segmentation might be further increased using this framework, which will be connected with the present clinical procedure and provide thorough treatment planning.

3. Proposed Methodology

This subsection describes the SAS optimization for calculating the decay parameter and the suggested MSRNet-3D with renal tumour image segmentation in 3D. In addition to optimizing several crucial model variables for increased performance and accuracy, this research aims to create and verify a novel DL structure for efficiently segmenting renal cancer pictures from 3D-CT. The integrated method builds comprehensive expertise in precise evaluation and planning of therapy for renal cancer by combining the capabilities of MSRNet-3D and SAS. The ability to capture multi-scale and multiple-level characteristics in 3D healthcare imaging data makes MSRNet-3D unique. Complex spatial interactions in 3D volumetric images are beyond the scope of traditional segmentation algorithms.

By using a hierarchy that incorporates feature gathering and processing at various scales along with levels, MSRNet-3D overcomes these constraints. Reliable segmentation and in-depth renal tissue analysis are features of the hierarchical architecture. It entails thorough segmentation and examination of renal tissue. The use of underlying 3D convolutions preserves the dimensional accuracy of the provided data, assisting the digestive tract models in accurately identifying and segmenting malignancies. This is a crucial component in effectively detecting renal cancer. The major input for the MSRNet-3D stream is 3D-CT images, which are contrast-stretched and standardized. The fundamental network, which has additional layers of 3D convolutions that extract the work's characteristics from fine towards coarse-scale data, is then run using the pre-processed photos. While methods like pooling reduce dimensionality, algorithms like ReLU improve non-linear translation. The segmentation overlay is then provided by the Segmentation Head, which is made up of convolutional neural networks, upsampling, and activation layers. Because this mask highlights locations of interest, like tumours, its categorization map is useful for additional research.

To achieve optimal performance in terms of segmentation accuracy, the MSRNet-3D model construction procedure involves a number of crucial parameters along with settings. Considerable experimentation adjusts this learning rate, resulting in a trade-off between precision and rapid convergence. The network can accurately distinguish between tumour regions and healthy tissues due to the application of the cross-entropy impairment

function categories, which closely match the multi-class character of tumour segmentation. Additionally, regularization of dropouts between layers is added from 0.3 to 0.5, avoiding overfitting and improving the model's capability to generalize to additional datasets. By levelling feature patterns of distribution, sequential normalization after compression improves the model's resilience and stabilizes learning while accelerating convergence. Multiple convolution levels with a kernel measurement of 3 × 3 are recommended for the segmentation network to capture complicated spatial characteristics. Pooling is added to decrease dimensionality, which conserves the important information. To maintain fine-grained information, particularly for the precise boundary identification of tiny or shaped differently tumours, skip connections are added to the model, significantly enriching it.

In order to capture sufficient information regarding context, this study suggests a framework that handles volumetric 3D data with a starting patch size of 128 × 128 × 64 that fits into Graphics Processing Unit (GPU) memory efficiently. The optimum segmentation accuracy will be achieved by further fine-tuning the weight decay using SAS, which will improve generalization to various clinical datasets. The MSRNet-3D model addresses key issues in renal cancer categorization with its modern capabilities and meticulously adjusted parameters, contributing to more precise and dependable diagnostic procedures, as shown in Figure 1.

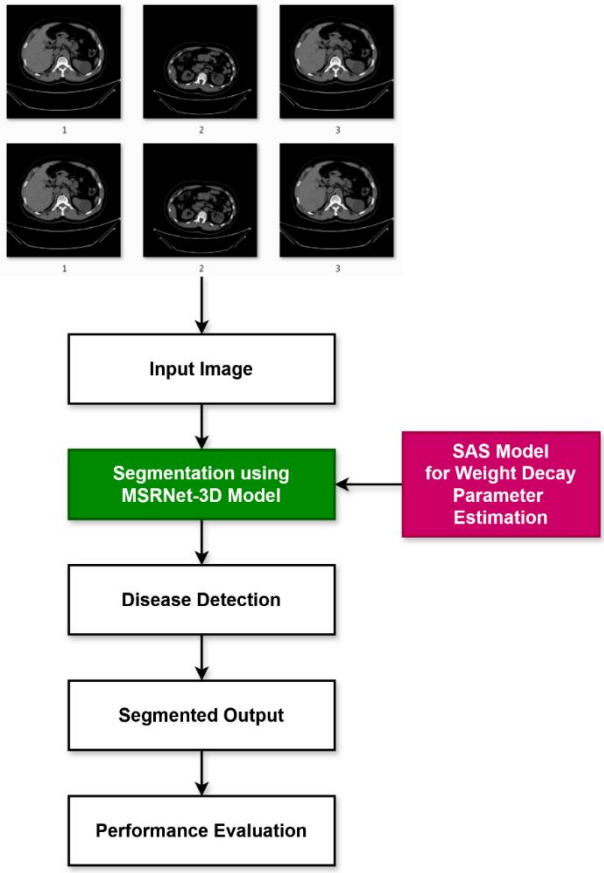

Fig. 1 Flow diagram of proposed MSRNet-3D tactic

The SAS Optimizing modifies the weighted decay variable, a crucial aspect of the model's capacity for generalization, in tandem with the segmentation evaluation. One of the important elements for a neural network's real-world expansion is weight degradation. Predicting performance is a huge undertaking, and a precise estimation of variables throughout a training session can prevent model overfitting and improve the learnt model's adaptation to fresh data. The decay factor is estimated by modifying the SAS optimization procedure's search variability. This makes it possible to create reliable and effective models that function well in a wide range of

applications, from autonomous systems to healthcare imaging. When predicting a time-to-event decay aspect, SAS yields more valid and responsible answers than a system that could have performed well in data from training but terribly in an observed test. Critical applications require this; for instance, a patient would require model identification of renal cancer disorders since the inaccuracy and unreliability could have serious repercussions. The SAS method was created by utilizing the capacity of sea horses to search and find in space optimization under spiral and Brownian motion types. The population's members also represent potential remedies; each one is given a fitness score based on certain limits. The adjustable and interpretive nature of SAS, hierarchical extraction of features, and volumetric analysis help the current MSRNet-Renal cancer be accurately and successfully diagnosed with 3D. In addition to improving the model's classification efficiency, this kind of integration ensures that the exact model is fine-tuned to capture the variability frequently found in renal cancer diagnostic data, improving early detection and efficient treatment planning.

3.1. Multi-Scale RenalNet 3D (MSRNet-3D)

One of the DL-based algorithms and architectures that have been taken into consideration for renal cancer classification and segmentation using 3D medical pictures is the MSRNet-3D methodology. Using convolution, the framework incorporates many scales and characteristics into 3D networks to provide a comprehensive 3D characteristic overview of renal malignant tissue. Multi-Scale RenalNet 3D enables the extraction of characteristics in a multi-scale system to make maximum use of highly unpredictable input at many granular levels. The first set includes a detailed extraction of the convolutional and textural layers, including edge attributes. The next layers provide a method for extracting even sharper, along with additional abstract characteristics. The architecture used in this study provides a foundation for localized, tiny characteristics and, more importantly, global structures common in 3D medical pictures.

The network's multiple-stage structure is linked to hierarchical recognition of features, which uses a set of layers, one for pooling and another for convolution. For the model to understand the context in which each feature resides with respect to the entire image, other network segments analyse the information supplied at various resolutions. This characteristic of the main factor in this categorization of processing distinguishes and divides between healthy and malignant portions based on minuscule differences in texture or structure. 3D convolutional layers are used in MSRNet-3D to handle volumetric data. While 3D convolution considers the spatial connection throughout all three dimensions, traditional 2D convolution processes, such as segments of 3D images, are disconnected from each other. This appears noteworthy when applied to clinical pictures to address contextual and architectural consistency, which are essential for drawing conclusions. Better detection of spatially complicated interactions in the renal cells might result from this, after a few tens of convolutional layers along with pooling frameworks, the input layer of MSRNet-3D processes 3D medical images. Likewise, each level receives input from the 2D net, which includes two convolutional layers that are activated with ReLU activations. These are subsequently followed through the pooling layers, which in this instance preserve the most important central properties while reducing their dimension with regard to the physical dimensions.

As a result, MSRNet-3D appears to be one of the significant developments in medical image processing, providing a useful and precise instrument for identifying cancer and, consequently, enhancing outcomes for patients. For pictures using 3D CT scans for the diagnosis of renal cancer, the suggested technique applies a Contextual Multi-Scale Multi-Level Network in conjunction with a 3D Convolutional Neural Network to achieve more accurate segmentation. This will enable more accurate segmentation by capturing local and global contextual data across a wide range of scales and levels. A CT scan with dimensions of P×Q×R is provided as the network's input, where P, Q, and R stand for the dimensions of the original image. Equation 1 illustrates how the features of the image at various scales are first removed when the input is received in order to obtain either fine or coarse details, as given in Equation 1.

$$\mathcal{E}_{s_i} = \mathcal{F}_{s_i}(\mathbb{I}), i \in \{1, 2, 3 \dots N\} \quad (1)$$

Where in $\mathbb{I}$ is the input 3D picture, $\mathcal{E}_{s_i}$ is the retrieved set of features, and $\mathcal{F}_{s_i}$ are the acquired features at scale i. In order to obtain structured information, a multi-level feature identification procedure is used, in which every level feature is analyzed at several scales. Equation 2 provides a mathematical representation of this procedure, which is given in equation 2.

$$\mathcal{E}_{l_j}^{s_i} = \mathcal{F}_{l_j}^{s_i}(\mathcal{E}_{s_i}), j \in \{1,2,3 \dots M\} \quad (2)$$

Where $\mathcal{E}_{l_j}^{s_i}$ denotes the obtained characteristics at multiple levels and $\mathcal{F}_{l_j}^{s_i}$ denotes the feature retrieval at level j. To obtain the greatest amount of characteristics extracted that correspond to the data for space in all three dimensions, the 3D convolutional layer procedure is then carried out. It can be expressed as follows in equation 3:

$$\mathcal{E}_{conv}^{s_i} = \text{Conv } 3D(\mathcal{E}_{l_M}^{s_i}) \quad (3)$$

And the 3D convolution procedure is represented by Conv 3D(.). Additionally, characteristics from different levels and scales are incorporated using the contextual integration method to provide a full feature representation, as illustrated in equation 4.

$$\mathcal{E}_{ctxt} = \sum_{i=1}^{N} \sum_{j=1}^{M} \mathcal{w}_{ij} \mathcal{E}_{l_j}^{s_i} \quad (4)$$

Whereas the weights that can be learned are used for integrating features from various scales and levels, are denoted by $\mathcal{w}_{ij}$. At the assumption of the procedure, the segmenting head procedure is used to build the ultimate segmentation mask by combining all of the characteristics. Equation 5 depicts it.

$$\mathcal{S} = \text{Segmentation Head}(\mathcal{E}_{ctxt}) \quad (5)$$

The segmented mask is denoted by S. In order to apply further processing to the improved characteristics for more efficient analysis and enhancement, the output is first run through the subsequent 3D convolutional procedure $\mathcal{E}_{conv}(p, q, r, h)$ once the Segmentation Head has been calculated. The size of the applied filter depends on the input volume. In this case, b is the bias factor for the h-th filter, and $\mathcal{w}_{i,j,l,h}$ represent the filter values. The convolution process creates the output characteristic maps, which exploit the input volume, integrate the learnt weights and biases, and take the weighted sum of the input dimension I at every spatial point (p,q,r).

This is particularly crucial for tasks like renal cancer identification, where the boundaries must be precisely demonstrated for proper evaluation and treatment. The framework can use the specifics to improve the reliability and specificity of the segmentation method by capturing complex designs and characteristics globally in an input size. Next, as indicated by equation 6, the 3D convolution procedure $\mathfrak{F}_{conv}(p, q, r, h)$ is carried out in equation 6.

$$\mathcal{E}_{conv}(p, q, r, h) = \sum_{i=1}^{\mathfrak{d}} \sum_{j=1}^{k} \sum_{l-1}^{w} \mathcal{w}_{i,j,l,h} \times \mathbb{I}_{c+i-1,v+j-1,y+l-1} + \mathcal{b}_h \quad (6)$$

Where $\mathcal{w}_{i,j,l,h}$ is the coefficient of the filter dimensions, $\mathcal{b}_h$ is the bias phrase, h is the source index within the convolutional layer, and (c,v,y) stands for the physical coordinates. Equation 7 is subsequently employed for approximating the activation parameter for ReLU, which strengthens the system by learning complex designs, including variations that are produced in Equation 7.

$$\varphi(c) = \max(0, c) \quad (7)$$

Additionally, as indicated in equation 8, the greatest possible pooling procedure is used for sampling down the inputs by obtaining the greatest number within a frame.

$$\mathrm{Max}_{\mathrm{pool}}(c, v, y, h) = \max_{i,j,l}, £_{c+i,v+j,y+l,h} \quad (8)$$

Next, using the following equation 9, the input's geographic complexity has been enhanced.

$$\mathcal{U}(p', q', r', h) = £([sp', sq', sr', h]) \quad (9)$$

Whereby the upsampling procedure is indicated by $\mathcal{U}(.)$. Additionally, the activations are normalized based on the information from the preceding layer using batch standardization, which greatly increases training speed and reliability. Equation 10 offers a mathematical representation of this operation.

$$\hat{a}^{(h)} = \frac{a^{(h)} - \mu^{(h)}}{\sqrt{(\sigma^h)^2 + \varepsilon}} \quad (10)$$

The amounts of activation associated with the hth channel are represented by $a^{(h)}$, the mean among the activations is $\mu^{(h)}$, the variability of the activity is shown by $(\sigma^h)^2$, and the tiny constant is represented by ε. Additionally, the detection procedure is much improved by the estimation of the gradient descent update rule using the optimal weight decay parameter. Equation 11, which is listed below, provides a mathematical representation of it.

$$\rho \leftarrow \rho - \delta(\Delta_\rho L + \beta\rho) \quad (11)$$

Where β stands for the amount of weight decay parameter, L for the loss process, δ for the learning percentage, and ϱ for the weights. The weight decaying ratio is ideally calculated in the proposed research with SAS. Renal malignancy identification will be significantly enhanced by the use of the MSRNet-3D framework in conjunction with 3D-CT image processing. For precise and thorough renal structure segmentation, a new model integrated the advantages of multi-scale and multi-level extraction of characteristics in the configuration of a 3D convolutional network. Effective tumour recognition and delineation are made possible by 3D convolutions' accurate spatial detail and dimensional authenticity, which are sufficient to guarantee excellent diagnostic precision. As a result, MSRNet-3D is a very powerful and dependable tool for targeting early identification and treatment preparation phases of renal cancer, improving patient outcomes. The framework's variables and their descriptions are shown in Table 1.

Table 1. Model parameters

Parameters	Description
$P \times Q \times R$	Image dimension
$\mathscr{f}_{s_i}$	Obtained features
$\mathbb{I}$	Input 3D image
$£_{s_i}$	Extracted features
$£_{l_j}^{s_i}$	Obtained multi-level features
$\mathrm{Conv}\ 3D(.)$	3D convolution operation
w_{ij}	Learnable weight
$\mathcal{S}$	Segmented mask
$\mathscr{b}$	Bias
(c, v, y)	Spatial coefficients

$\mathcal{U}(.)$	Upsampling operation
$a^{(h)}$	Activation function
$\mu^{(h)}$	Mean of activation
δ	Learning rate
L	Loss function
β	Weight decay

3.2. Seahorse Adaptive Search (SAS) Optimization for Deterioration Factor Estimation

Focusing on seahorses' hunting and adaptability skills, the Seahorse Adaptive Search (SAS) Optimization approach is a novel search methodology. Regarding the details of decay factor assessment, SAS offers a somewhat reasonable and practical method for addressing one of the main problems in neural networks, along with machine learning. The "decay factor," a method of regularizing weights that diminishes over-fitting by "fining" big weights throughout training, is typically assigned weight decay. Because the decay parameter affects the model's capacity to generalize to new data and increase its accuracy and stability, it should be accurately evaluated. The SAS Optimization approach closely examines the precision of the seahorse variation selection approach in its methodology. Thanks to their exceptional movement control, seahorses can seek, capture, and manoeuvre in water situations. Concerning searching and exploiting, the overall outcome is fine-grained due to the SAS algorithm's flexibility in the search area. In contrast to other optimization strategies, the significance of this process allows SAS to investigate the proper decay factor while retaining the capacity to exploit.

The importance of using SAS to determine the decay factor cannot be overstated. One of the most important factors in implementing and training neural networks involves the decay factor that establishes how resistant the framework is to overfitting. Instead of just recurrently learning the sets, a framework with an optimal decay factor value can identify patterns in the data used as training. This is especially true for applications like medical image analysis, where models must function well with data never used for training. The provided example of utilizing SAS to calculate the decay factor shows that researchers and practitioners can discover improved and more accurate factor evaluation through the software's dependability, leading to more effective and dependable models. When applied to fields like finance, health, and especially autonomous system development, the potential for fine-tuning the degradation factor exploiting SAS would greatly outweigh the performance gains of DL models. The second positive thing is that SAS allows you to modify the regularization variable, which allows you to achieve much more precision for a more reliable training procedure, which ultimately results in a decent model. An effective adaptive method for calculating the decay parameter is the most novel aspect of the SAS optimization strategy. In regard to model dependability, it provides scores and graphically illustrates advantages above traditional approaches that can be used in machine learning approaches.

Algorithm 1 – SAS based Weight Decay Parameter Estimation

Step 1: //Parameter initialization;
Amount of iterations, population size, upper and lower boundaries, and constant factor.

Step 2: For every person in the population
Update the position is given in Equations 12 and 13.

$$S_i = [s_i^1, s_i^2 \dots s_i^d] \quad (12)$$

$$s_i^j = \tau \times \left(ub_j - lb_j\right) + lb_j \quad (13)$$

//Where, S_i – Set of population, i – individual, j – dimension, τ – random parameter, lb_j – lower bound, and ub_j – upper bound;

Step 3: Determine each person's fitness function.
Step 4: Identify the elite person as indicated below in equation 14.

$$S_{elite} = \arg\min(\mathcal{F}(s_i)) \quad (14)$$

//Where, $\mathcal{F}(s_i)$ – Fitness function;
Step 5: For (itr to mx_{itr})
Perform spiral motion;
Update position;
Step 6: Perform Brownian motion;
Update position;
End for;
Step 7: Perform the movement update given in equation 15.

$$S_{nw}^{(1)}(itr+1) = \begin{cases} S_i(itr) + Levy(\mathcal{k})((S_{elite}(itr) - S_i(itr)) \times s \times g \times h + S_{elite}(itr)) \\ S_i(itr) + \tau \times \gamma_{itr} \times (S_i(itr) - \gamma_{itr} \times S_{elite}) \end{cases} \quad (15)$$

Step 8: Carry out breeding behaviour and predation activities.
Step 9: Modify the population
Step 10: As seen here, update fitness with an outstanding individual in Equation 16.

$$S_{elite} = \arg\min(\mathcal{F}(s_i)) \quad (16)$$

Step 11: Return S_{elite};

In this research, the SAS approach, a consistently effective technique to maximise the weight parameters in DL models, is used to estimate the weight decay variable. The SAS method effectively searches the solution set by utilizing the seahorse's distinctive actions, including spiral and Brownian motion. Because the approach is responsive and balances exploration and exploitation, this may be guaranteed while searching for the right weight decay values. This algorithm's ability to break out of local minima and adjust to a changing environment of additional optimization issues is quite remarkable. In many situations, it is clearly a powerful tool that simplifies the customization of relatively complicated frameworks.

4. Results and Discussion

The new MSRNet-3D model's efficiency is assessed, and its outcomes are contrasted with a number of diversity metrics. Since it requires precise categorization, the MSRNet-3D model's identification of renal tumours from 3D-CT images constitutes one of the most revolutionary advancements in medical image processing. The effectiveness of the suggested framework for multi-metrics was further examined using the KiTs19 dataset, which included vascular CT images from 210 individuals. Therefore, these studies measure the precision, reliability, and clinical usefulness of properly and efficiently defining renal regions and detecting particular renal mass categories. This introduction lays the groundwork for the discussion of the MSRNet-3D model's performance assessment, highlighting the necessity for its excellent clinical outcomes and demonstrating its application to a large dataset.

The KiTs19 dataset represents one of the important resources in medical imaging, particularly regarding vascular CT for nephrectomy techniques in the removal of renal masses. More precisely, it was carefully selected from the broad public domain 2019 Medical Image Computing and Computer Assisted Intervention (MICCAI) renal cancer segmentation competition training set, which included 210 3D-CT scans comprising 210 patients. In order to provide a broad understanding of the majority of renal diseases, these cases were selected to represent a variety of renal cancer types. Clear cell RCC is the diagnosis made for most of the 210 scans comprising this dataset.

RCC is a regularly occurring category of renal cancer that exhibits a variety of clinical symptoms according to its histopathological characteristics.

The KiTs19 dataset represents one of the fundamental resources in the field of medical imaging, particularly with regard to vascular CT for nephrectomy techniques in the removal of renal masses. More precisely, it was carefully selected from the broad public domain 2019 Medical Image Computing and Computer Assisted Intervention (MICCAI) renal cancer segmentation competition training set, which included 210 3D-CT scans comprising 210 patients. In order to provide a broad understanding of the majority of renal diseases, these cases were selected to represent a variety of renal cancer types. Clear cell RCC is the diagnosis made for the majority of the 210 scans that comprise this dataset. RCC is a frequently occurring category of renal cancer that exhibits a variety of clinical symptoms according to its pathological characteristics. Because they enable radiologists to make precise diagnoses and oncologists to track treatment outcomes and pre-operative planning for individuals with renal masses, these models will be essential for clinical use. In addition to serving as a benchmarking framework for segmentation methods, the KiTS19 dataset makes a significant contribution to future studies in computerized diagnosis, including medical picture analysis. In this way, datasets can be used to progress novel strategies for improving renal tumour segmentations' accuracy, effectiveness, and repeatability to improve patient outcomes and clinical judgment in radiological and oncological treatment. For the recommended MSRNet-3D approach, Figure 2 displays the ground reality and segmented pictures of renal carcinoma based on the KiTS19 dataset.

It specifically demonstrates how accurately the model defined the areas of renal carcinoma that were also present in the physical truth. The two images throughout the figure are essentially a categorized output image from MSRNet-3D and a genuine ground truth image. The results demonstrate that MSRNet-3D can exactly identify and segment renal cancer areas in arterial CT scans, producing segmentation results that closely resemble expert-annotated genuine data. The strong performance of this framework for its possible application in a clinical environment for exacting renal tumour detection and diagnosis may be supported by this unstructured or visual verification.

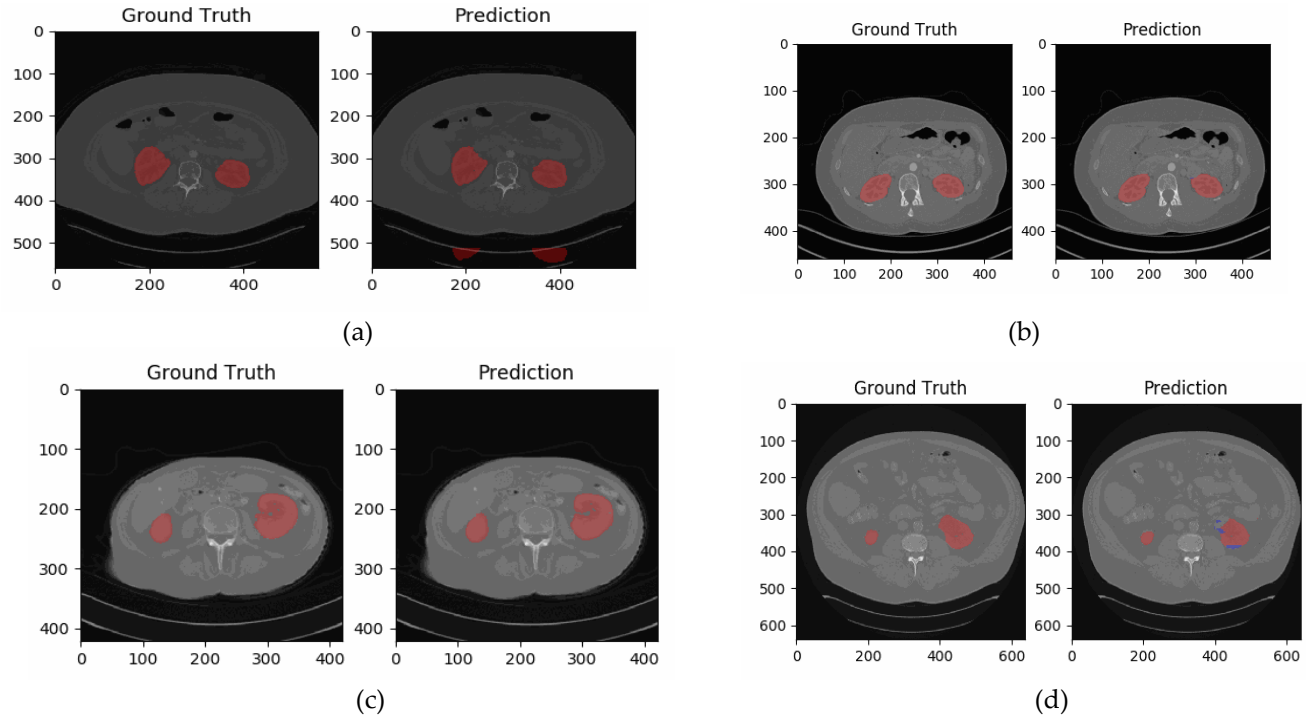

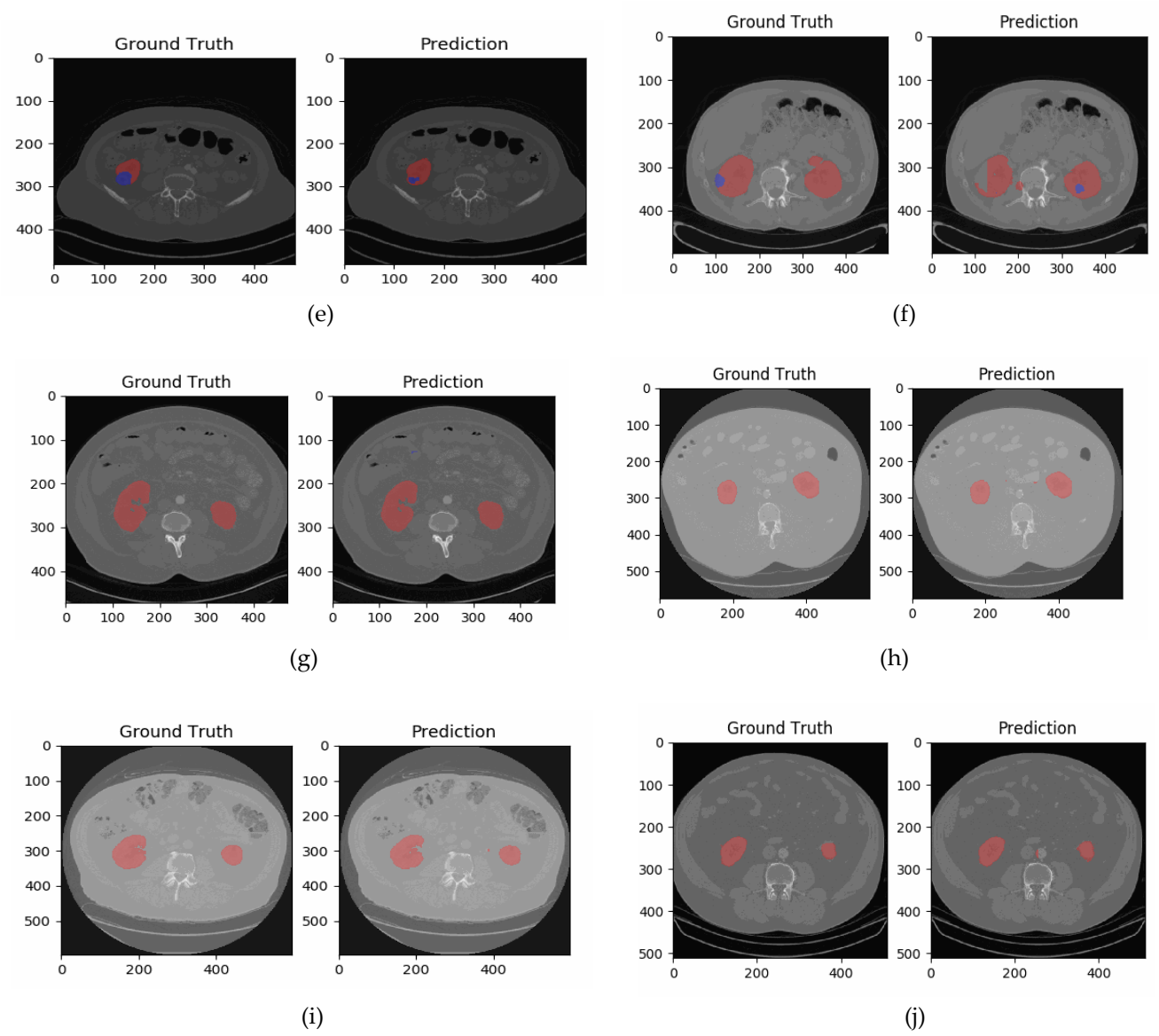

Fig. 2(a-j) Ground truth and expected images

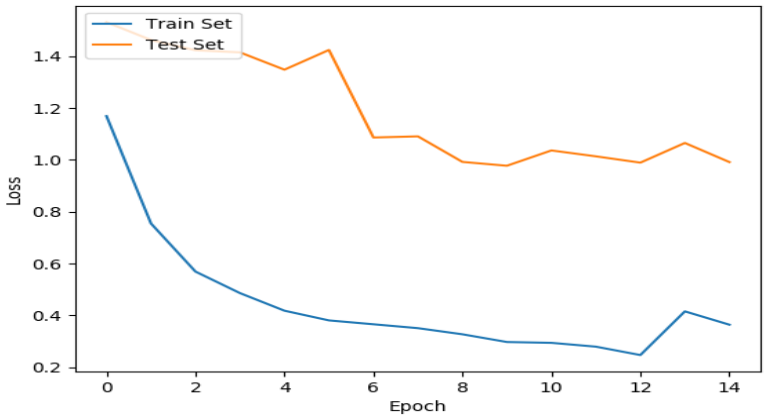

Fig. 3 Training and testing loss

The acquired model, MSRNet-3D's testing and training loss curves are displayed in Figure 3. The difference between the anticipated values and the actual truth is plotted across successive training epochs to create a graph representing the loss. The framework learns to make fewer errors on the data used for training, as evidenced by the training curve almost always moving downward. A dependable or lower testing loss and the training loss suggest that the model continues to learn well without excessively fitting the existing training data; therefore, it will adapt well to new data. On the other hand, the testing loss curve scores the model's accuracy against undetectable validation data to demonstrate its ability for generalization.

Fig. 4 Dice coefficient when training

The dice parameter scores following the MSR-Net-3D training of models are displayed in Figure 4. The Dice value is a frequently used metric for assessing the degree of overlapping and resemblance between a segmentation output and real-world layers in medical picture segmentation assignments. Greater consistency between a model's prediction and the actual segmentation masks is indicated by a higher Dice correlation value, which suggests that the framework is effective in identifying renal cancer areas from 3D-CT images. This investigation demonstrates the model's precision in segmentation in accurately recognizing and demarcating renal tumour areas.

The MSRNet-3D strategy's overall effectiveness in the procedure for segmentation of the vascular CT images obtained from the KiTs19 dataset is demonstrated by Table 2 and Figure 5, which show the accuracy of the model research across multiple sub-classes of renal tumours. Area Under the Curve (AUC), Specificity, Sensitivity, and other important parameters are used to evaluate each subclass, including Clear Cell, Papillary, Chromophobe, Oncocytoma, and others. Given that its matching AUC values range from 98.5% to 99.2%, the U-net MSRNet-3D model performs exceptionally well across all categories.

In particular, high specificity scores highlight its ability to identify the so-called genuine negatives, the majority of the time. When it comes to identifying what are considered “true positives,” its sensitivity score ranges from 98.2% to 99.1%, demonstrating good robustness. These outcomes showed how well the MSRNet-3D model could differentiate between different kinds of renal malignancies, enabling trustworthy segmentation as well as classification in a healthcare setting.

Table 2. Performance evaluation with reference to diverse classes

Subclass	AUC	Specificity	Sensitivity
Clear cell	98.5	98.3	98.2
Papillary	99	98.9	98.8
Chromophobe	99.2	99	99.1
Oncocytoma	99.1	98.8	98.8
Others	98.9	98.8	98.6

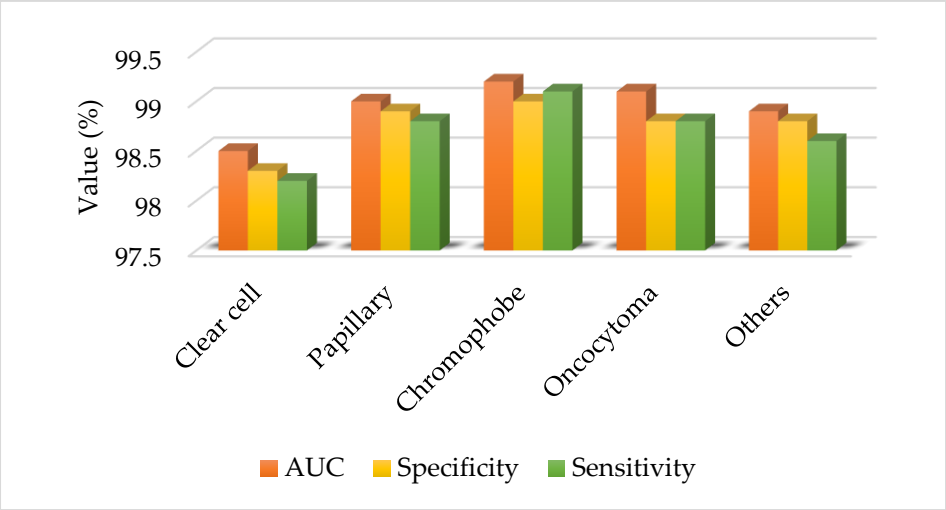

Fig. 5 Performance examination of the proposed MSRNet-3D tactic

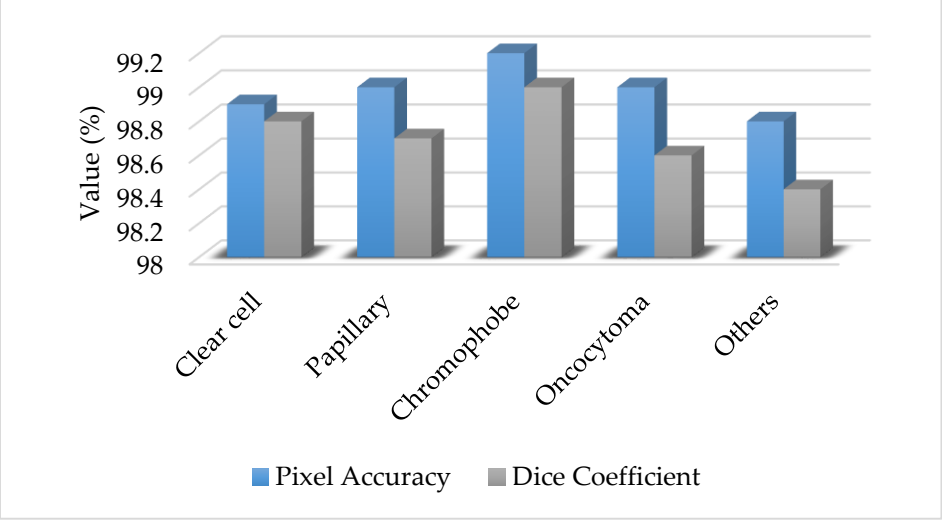

Fig. 6 Performance exploration of the proposed MSRNet-3D model related to pixel accuracy and dice coefficient

Table 3. Performance related to pixel accuracy, dice coefficient

Subclass	Pixel Accuracy	Dice Coefficient
Clear cell	98.9	98.8
Papillary	99	98.7
Chromophobe	99.2	99
Oncocytoma	99	98.6
Others	98.8	98.4

A detailed examination of the MSRNet-3D strategy evaluation outcomes, encompassing the dimension accuracy as well as Dice coefficient for each type of renal cancer subtype, is shown in Table 3. Five subclasses, clear cell, papillary, chromophobe, oncocytoma, and other kinds, are evaluated in the table using the coefficient of Dice and the two discriminatory metrics of pixel consistency. The MSRNet-3D demonstrated accuracy levels of roughly 98.8% to 99.2%. Pixel accuracy is the percentage of accurately categorized pixels in the segmentation masks that the model creates. The framework's capacity to segment tumour boundaries is further demonstrated by the Dice coefficient, which quantifies the overlap between the ground truth and the predicted segmentation mask. When contrasted with scores ranging from 98.4% to 99%, the difference in the dice coefficient values evaluated for the MSRNet-3D model shows an exceptional efficiency. These outcomes demonstrate the model's practical utility in medical imaging operations by reliably demonstrating its capacity to separate renal cancers according to their respective histological categories.

Figure 6 shows the bar representation of the MSRNet-3D strategy performance analysis related to pixel consistency and dice coefficient, in addition to Table 3. The picture simply addresses the fourth hypothesis of the article by equalling the predicted Dice coefficient and pixel consistency for different renal carcinoma subcategories. Clear cell, papillary, chromophobe, oncocytoma, and different tumour types are represented by each bar in the graphic, which also precisely repeats the model's MSRNet-3D in the segmentation processes. Its capacity to outline the tumour borders, especially, is further enhanced by the representation of these measurements in Figure 7, which suggests a higher likelihood of accurate diagnosis and improved therapy planning as an actual utilization of the framework in healthcare.

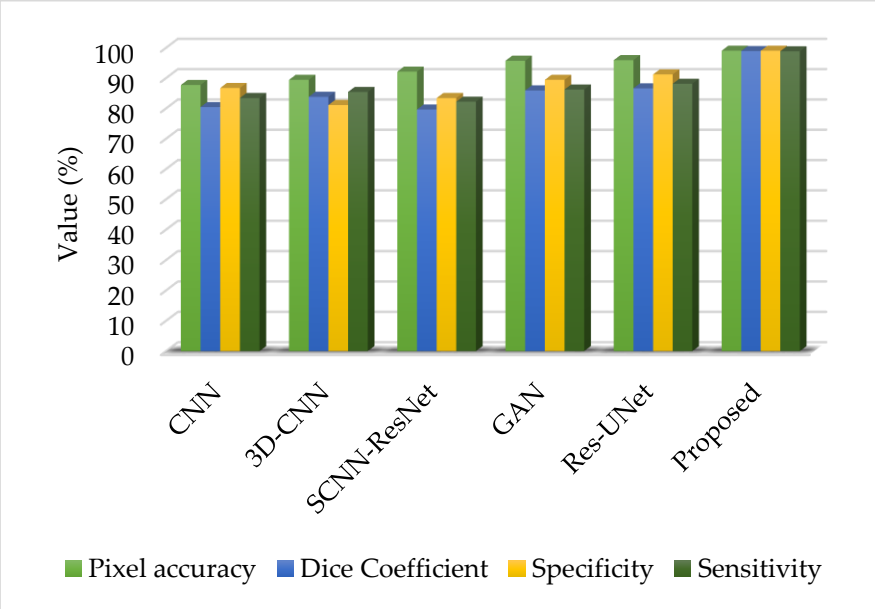

Fig. 7 Assessment based on pixel accuracy and dice similarity portion

Table 4. Contrast with state-of-the-art approaches

Methods	Pixel accuracy	Dice Coefficient	Specificity	Sensitivity
CNN	87.7	80.4	86.7	83.4
3D-CNN	89.4	83.8	81.1	85.4
SCNN-ResNet	92.1	79.6	83.4	82.2
GAN	95.7	85.9	89.4	86.2
Res-UNet	95.9	86.6	91.2	88.1
Proposed	99	98.9	99	98.8

Additionally, Table 4 contrasts the suggested MSRNet-3D algorithm with alternative medical imaging methods for segmentation. The conventional method, CNNs, 3D CNNs, Statistical Convolutional Neural Network (SCNN)-ResNet, Generative Adversarial Network (GAN), depending techniques like Fully Convolutional Network (FCN), Res-UNet, along with the recently released MSRNet-3D framework, are among the methods whose pixel accuracy, along with Dice coefficient, are compared in the table. The effectiveness of each process is assessed based on its ability to segment renal tumours accurately. The results showed an improvement in segmentation accuracy and reliability. In particular, it is significant that the suggested MSRNet-3D model achieves the best results, with an individual pixel precision of 99% and a dice factor of 98%. The higher effectiveness of MSRNet-3D in defining the tumour boundaries and the possibility for it to enhance diagnostic accuracy in clinical practice are indicated by these scores, which outperform all other targeted approaches mentioned.

It provides a visual representation of how well various segmentation techniques work based on the Dice coefficient and pixel consistency. The comparative examination of all the approaches on those variables is presented in Figure 8, highlighting the distinctiveness of the MSRNet-3D model in comparison to CNNs, 3D-CNNs, SCNN-ResNet, GAN, along with Res-UNet. A convenient evaluation of the segmentation effectiveness of the various approaches is provided by the figures, which are displayed as a bar with the pixel precision and Dice index displayed. The MSRNet-3D obtained good scores for both measurements, indicating that the suggested approach efficiently produces accurate and reliable segmentation results. This suggests that the model may play a part in enhancing renal tumour evaluation through the use of cutting-edge medical imaging techniques. The suggested MSRNet-3D models' specificity and sensitivity parameters for medical picture segmentation are compared to a number of cutting-edge segmentation algorithms. The metrics take into consideration how well or poorly the segmentation approach in question classifies any specific test case as either positive or negative. For example, renal tumour identification is measured by sensitivity, a feature of genuine positives, and specificity, which is the percentage of true negatives. With an accuracy of 98.8% along with a specificity score of 99%, the analysis that is supplied performs best. The techniques list, which includes conventional CNNs, 3D-CNNs, SCNN-ResNet, GAN-based approaches, and Res-UNet, is topped by these noticeably superior findings.

Furthermore, connection bypassing, continuous normalization, and dropping regularization have enhanced model fitting and approach generalization, making the suggested model suitable for a range of datasets as well as clinical settings. MSRNet-3D's versatility among tumour subtypes and anatomical complexity suggests more adaptability, providing doctors with interpretable data in simple workflows. However, the research is limited in that it heavily relies on computer resources over inferences and training, which makes it even less feasible for clinical practice with limited resources. Furthermore, even if the performance is good across all evaluated datasets, scalability and consistency ought to be guaranteed by further authentication on multi-scale datasets with more accurate characteristics of patients. Similarly, areas without access to high-quality imaging data could find it difficult to train utilizing a lot of annotated datasets. Notwithstanding these drawbacks, the suggested MSRNet-3D model is a revolutionary advancement in the segmentation of renal cancer and lays the groundwork for future advancements and oncology uses in medicine.

5. Conclusion

By addressing important shortcomings of current models, including varying accuracy, imprecision, and insufficient response to complex tumour characteristics, the proposed Multi-Scale RenalNet 3D (MSRNet-3D) offers a substantial leap in renal cancer segmentation. MSRNet-3D significantly improves segmentation precision and reliability across various datasets by utilizing the SAS approach for weight decay improvement. This enhancement makes it easier to identify and categorize renal tumours with more accuracy, giving medical professionals clearer, easier-to-understand 3D representations they need for efficient evaluation and preparation of treatment. It has encouraging potential for widespread clinical use due to its scalability and resilience across a range of patient demographics and imaging circumstances. According to experimental results, the model's unmatched capacity for

tumour detection and delineation to an exceptionally high level of precision is established by its 99% accuracy rate, 98.9% accuracy, and 99% recall. MSRNet-3D's F1-score, which gauges performance in terms of recall as well as accuracy, was 98.8%. The model will be refined through future evaluation utilizing multi-centre datasets, improving its interpretability and facilitating its seamless incorporation into clinical workflows in a real-time environment.

Ethical Statement

I will conduct myself with integrity, fidelity, and honesty. I will openly take responsibility for my actions and only make agreements I intend to keep. I will not intentionally engage in or participate in malicious harm to another person or animal.

References

[1] Zhuo Chen et al., "Comprehensive 3D Analysis of the Renal System and Stones: Segmenting and Registering Non-Contrast and Contrast Computed Tomography Images," *Information Systems Frontiers*, vol. 27, no. 1, pp. 97-111, 2024. [CrossRef] [Google Scholar] [Publisher Link]

[2] Vinitkumar Vasantbhai Patel et al., "A Systematic Renal Tumor Segmentation and Classification Framework using Adaptive and Attentive-based Deep Learning Networks with Improved Crayfish Optimization Algorithm," *IEEE Access*, vol. 12, pp. 85635-85660, 2024. [CrossRef] [Google Scholar] [Publisher Link]

[3] Marie-France Bellin et al., "Update on Renal Cell Carcinoma Diagnosis with Novel Imaging Approaches," *Cancers*, vol. 16, no. 10, pp. 1-33, 2024. [CrossRef] [Google Scholar] [Publisher Link]

[4] Xun Zhao et al., "The Application of CT Radiomics in the Diagnosis of Vein Wall Invasion in Patients with Renal Cell Carcinoma Combined with Tumor Thrombus," *The Oncologist*, vol. 29, no. 2, pp. 151-158, 2024. [CrossRef] [Google Scholar] [Publisher Link]

[5] ChengWei Fu et al., "Using Three-Dimensional Model-Based Tumour Volume Change to Predict the Symptom Improvement in Patients with Renal Cell Cancer," *3 Biotech*, vol. 14, no. 5, pp. 1-8, 2024. [CrossRef] [Google Scholar] [Publisher Link]

[6] Suping Yanget al., "Radiomics Analysis Based on Single Phase and Different Phase Combinations of Radiomics Features from Tri-Phasic CT to Distinguish Renal Oncocytoma from Chromophobe Renal Cell Carcinoma," *Abdominal Radiology*, vol. 49, no. 1, pp. 182-191, 2024. [CrossRef] [Google Scholar] [Publisher Link]

[7] Alex G. Raman et al., "Radiomics and Artificial Intelligence: Renal Cell Carcinoma," *Urologic Clinics*, vol. 51, no. 1, pp. 35-45, 2024. [CrossRef] [Google Scholar] [Publisher Link]

[8] R. Rajkumaret al., "DARKNET-53 Convolutional Neural Network-Based Image Processing for Breast Cancer Detection," *Mesopotamian Journal of Artificial Intelligence in Healthcare*, vol. 2024, pp. 59-68, 2024. [CrossRef] [Google Scholar] [Publisher Link]

[9] Maryamalsadat Mahootiha et al., "Multimodal Deep Learning for Personalized Renal Cell Carcinoma Prognosis: Integrating CT Imaging and Clinical Data," *Computer Methods and Programs in Biomedicine*, vol. 244, pp. 1-14, 2024. [CrossRef] [Google Scholar] [Publisher Link]

[10] Kwang-Hyun Uhm et al., "Lesion-Aware Cross-Phase Attention Network for Renal Tumor Subtype Classification on Multi-Phase CT Scans," *Computers in Biology and Medicine*, vol. 178, pp. 1-14, 2024. [CrossRef] [Google Scholar] [Publisher Link]

[11] Abeer J. Alhussaini et al., "Radiomics Machine Learning Analysis of Clear Cell Renal Cell Carcinoma for Tumour Grade Prediction Based on Intra-Tumoural Sub-Region Heterogeneity," *Cancers*, vol. 16, no. 4, pp. 1-35, 2024. [CrossRef] [Google Scholar] [Publisher Link]

[12] P. Suman Prakash et al., "Decoupled Sculptor GAN Framework for 3D Reconstruction and Enhanced Segmentation of Renal Tumors in CT Images," *IEEE Access*, vol. 12, pp. 62189-62198, 2024. [CrossRef] [Google Scholar] [Publisher Link]

[13] MM. Yaodan Zhang et al., "Preoperative Prediction of Renal Fibrous Capsule Invasion in Clear Cell Renal Cell Carcinoma Using CT-Based Radiomics Model," *British Journal of Radiology*, vol. 97, no. 1161, pp. 1557-1567, 2024. [CrossRef] [Google Scholar] [Publisher Link]

[14] Venkatesan Rajinikanth et al., "A Framework to Distinguish Healthy/Cancer Renal CT Images Using the Fused Deep Features," *Frontiers Public Health*, vol. 11, pp. 1-11, 2023. [CrossRef] [Google Scholar] [Publisher Link]

[15] G. Maheswari, and S. Gopalakrishnan, "Dynamic Channel Attention for Enhanced Spatial Feature Extraction in Medical Image Analysis using Advanced Attention Capsule Network," *2024 International Conference on Integrated Circuits and Communication Systems (ICICACS)*, Raichur, India, pp. 1-7, 2024. [CrossRef] [Google Scholar] [Publisher Link]

[16] Kai Wu et al., "A Comprehensive Texture Feature Analysis Framework of Renal Cell Carcinoma: Pathological, Prognostic, and Genomic Evaluation Based on CT Images," *European Radiology*, vol. 32, no. 4 pp. 2255-2265, 2022. [CrossRef] [Google Scholar] [Publisher Link]

[17] Jingya Liu et al., "AI-Driven Robust Renal and Renal Mass Segmentation and Classification on 3D CT Images," *Bioengineering*, vol. 10, no. 1, pp. 1-12, 2023. [CrossRef] [Google Scholar] [Publisher Link]

[18] Huancheng Yang et al., "An Automated Surgical Decision-Making Framework for Partial or Radical Nephrectomy Based on 3d-CT Multi-Level Anatomical Features in Renal Cell Carcinoma," *European Radiology*, vol. 33, no. 11, pp. 7532-7541, 2023. [CrossRef] [Google Scholar] [Publisher Link]

[19] Dhuha Abdalredha Kadhim, and Mazin Abed Mohammed, "A Comprehensive Review of Artificial Intelligence Approaches in Renal Cancer Medical Images Diagnosis, Datasets, Challenges and Issues and Future Directions," *International Journal of Mathematics, Statistics, and Computer Science*, vol. 2, pp. 199-243, 2024. [CrossRef] [Google Scholar] [Publisher Link]

[20] Kwang-Hyun Uhm et al., "Deep Learning for End-to-End kidney Cancer Diagnosis on Multi-Phase Abdominal Computed Tomography," *NPJ Precision Oncology*, vol. 5, no. 1, pp. 1-6, 2021. [CrossRef] [Google Scholar] [Publisher Link]

[21] Dalia Alzu'bi et al., "kidney Tumor Detection and Classification Based on Deep Learning Approaches: A New Dataset in CT Scans," *Journal of Healthcare Engineering*, vol. 2022, pp. 1-22, 2022. [CrossRef] [Google Scholar] [Publisher Link]

[22] Zhanlin Ji et al., "ASD-Net: A Novel U-Net Based Asymmetric Spatial-Channel Convolution Network for Precise kidney and kidney Tumor Image Segmentation," *Medical and Biological Engineering and Computing*, vol. 62, no. 6, pp. 1673-1687, 2024. [CrossRef] [Google Scholar] [Publisher Link]

[23] Maryamalsadat Mahootiha et al., "Deep Learning-Assisted Survival Prognosis in Renal Cancer: A CT Scan-Based Personalized Approach," *Heliyon*, vol. 10, no. 2, pp.1-15, 2024. [Google Scholar] [Publisher Link]

[24] Minpeng Jiang et al., "MDSK-Net: Multi-Scale Dynamic Segmentation Kernel Network for Renal Tumour Endoscopic Image Segmentation," *IET Image Processing*, vol. 18, no. 11, pp. 2855-2868, 2024. [CrossRef] [Google Scholar] [Publisher Link]

[25] Yu-Ning Feng et al., "Predictive Value of Computed Tomography Radiomics Combined with Traditional Imaging Features in WHO/ISUP Grading of Clear Cell Renal Carcinoma," *International Journal of Imaging Systems and Technology*, vol. 34, no. 3, 2024. [CrossRef] [Google Scholar] [Publisher Link]